Virtual Inertia Emulation using Commercial Off-The-Shelf Inverters

Ujjwol Tamrakar*, *IEEE Student Member*, Fernando B. dos Reis*, *IEEE Student Member*, André Luna*, Dipesh Shrestha[†], Robert Fourney*, *IEEE Member*, and Reinaldo Tonkoski*, *IEEE Member**Department of Electrical Engineering and Computer Science, South Dakota State University, Brookings, SD

†Primus Power, Hayward, CA

Email: ujjwol.tamrakar@jacks.sdstate.edu

Abstract—Virtual inertia based control of renewable energy sources (RESs) helps to enhance the frequency stability of power systems. In this paper, a Control Area Network (CAN) communication-based method is demonstrated to emulate virtual inertia using commercial off-the-shelf inverters. This allows the currently installed systems to be retrofitted with virtual inertia in a cost-effective manner which would allow for higher RES penetration in power systems. The proof-of-concept is demonstrated using a Xantrex XW6048 hybrid inverter/charger and OPAL-RT real-time digital simulator. Results show that CAN-based communication can be an effective way to reduce frequency variations in the power system.

Index Terms—Virtual inertia, CAN communication, Real-time digital simulation, frequency stability

I. INTRODUCTION

Recently, power systems have seen a substantial increase in power electronics based renewable energy sources (RESs). The mechanical inertial response in the power system is thus in continuous decline as the power electronics based RESs do not contribute to the system inertia. This has led to frequency stability issues in power systems [1]. This is particularly true for remote microgrids, as high RES penetration further reduces the inertia of an already weak system. Virtual inertia emulation through power electronic converters has been widely proposed in the literature as a possible solution to counteract the aforementioned frequency instability problems [2]–[4].

Microgrids have been identified as the best option to integrate distributed generation (DG) units in terms of flexibility and reliability [5], [6]. The microgrids can be operated in three possible modes: grid-connected, islanded or isolated. A microgrid is said to have been islanded when a microgrid that is grid-connected disconnects from the grid, either in a planned fashion or due to a fault/disturbance in the main grid. In the isolated mode of operation, the microgrid is designed such that it is never connected to the grid. Regardless, these microgrid systems represent weak power systems and the high penetration of inertia-less PV and wind energy systems has a severe effect on the frequency stability. The rapid changes in the generation can cause frequency variations in the system that are outside standard limits and compromise the stability of the system. From a generator point-of-view, frequency standards like the ISO 8528-5 standard [7] can provide a guideline for the frequency limits. With the small amount of SG in isolated microgrids, the frequency excursions and rateof-change-of-frequency (ROCOF) are greater and the need for virtual inertia is of high importance.

Retrofitting existing systems to incorporate virtual inertia can eliminate frequency instability in systems with high RES penetration. However, the fact that the firmware of commercial inverters cannot be easily modified is among the main barriers to the implementation of virtual inertia algorithms in existing power converters [8]. This paper discusses a communication system based approach using Control Area Network (CAN) communication to integrate virtual inertia-based control in commercial inverters in a cost-effective manner. As a proofof-concept, an OPAL-RT real-time digital simulator (RTDS) is used to implement the algorithm and establish communication with the commercial inverter. However, this concept can be easily implemented with simple and cheap controllers as well. A similar benchmark using CAN communication was developed in [8] for energy management systems of microgrids. This paper expands on the same benchmark, by exploring the possibility of using CAN communication for virtual inertia emulation which needs much faster communication speeds compared to the steady-state tests performed in [8].

This paper is organized as follows: Section II first gives the basic concept of the virtual inertia algorithm, the details of the CAN communication is given in Section III. The procedures and the experimental setup used for implementation of virtual inertia using a commercial inverter is described in Section IV. Section V presents some experimental results which is followed by the conclusions and future work in Section VI.

II. CONCEPT OF VIRTUAL INERTIA

Virtual inertia is a combination of RESs, energy storage systems (ESSs), power electronics, and a control algorithm which emulates inertia of a conventional power system [9]. The basic schematic illustrating the concept of virtual inertia is shown in Fig. 1. Typically, RESs such as wind, photovoltaics (PV), and even ESSs are interfaced to the grid as current sources without providing any inertial response. But with the virtual inertia algorithm, the power output of an inverter is controlled based on the frequency derivative and change in system frequency as:

$$P_{VI} = k_{inertia} \left(\frac{d\Delta f}{dt} \right) + k_{damp} \Delta f \tag{1}$$

where P_{VI} is the power injected/absorbed by the inverter, Δf is the change in system frequency, $\frac{d\Delta f}{dt}$ is the rate-of-change-of-frequency, $k_{inertia}$ is the inertia constant, and k_{damp} is the damping constant.

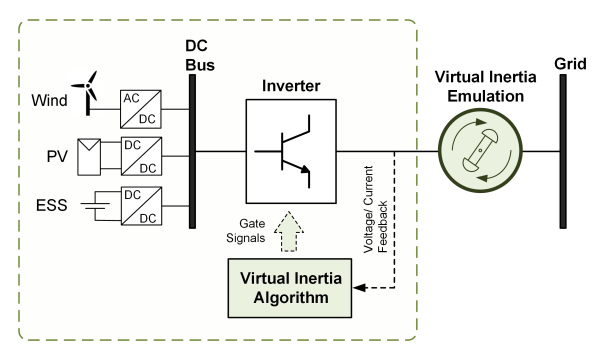


Fig. 1: Basic concept of virtual inertia.

The frequency of the system is usually measured using a phase-locked loop (PLL). Typically, frequency measurements have a lot of noise associated with it. So, a deadband is usually utilized when implementing virtual inertia systems so that the system does not respond to small variations in the system frequency. However, proper selection of this deadband is crucial for a virtual inertia system as it will be described later.

III. DETAILS OF CAN COMMUNICATION LINK

CAN is an advanced differential two-line serial communication network which transmits data in terms of sequences and packages and supports real-time control [10]. CAN-based networks have been widely used in the automotive industry and have been extended to other industrial environments as well [11]. This section describes the configuration used to setup the CAN communication and gives the details on how commands were sent on the CAN bus.

A. CAN Communication Setup

A CAN-AC2-PCI interface card from Softing as shown in Fig. 2 was used for establishing the bus interface between OPAL-RT RTDS and Xantrex inverter/charger. The CAN-AC2-PCI card had two channels and each of those channels were capable of communicating with up to 100 CAN nodes. Among these two channels, one of the channels was configured to send commands to the inverter/charger unit using a 9-pin D-Sub CAN bus. RT-LAB, the simulation software for OPAL-RT RTDS, provides all the blocks to setup CAN communication and send/receive CAN messages. The OPAL-RT connects through the CAN physical layer with ISO standard 11898-2 high-speed transmission with 120 Ω resistor connection to match the impedance of the physical layer. The bit transfer rate was set at 250 kbps. Unique and fixed message identifiers were used for data transmission. In this system, the identifier is followed by the data to be transmitted. Extended identifiers were used to control and command the Xantrex inverter/charger.

Figure 3 shows the block diagram of the CAN physical layer. CAN has a controller that controls and manages the

transmit and receive lines. These lines are then connected to the physical CAN bus through a CAN transceiver. Based on the frequency measurements received by the OPAL-RT system, power references are computed based on (1) which are then sent out as current commands to the Xantrex inverter using the CAN communication protocol.



Fig. 2: CAN-AC2-PCI card with two CAN channels.

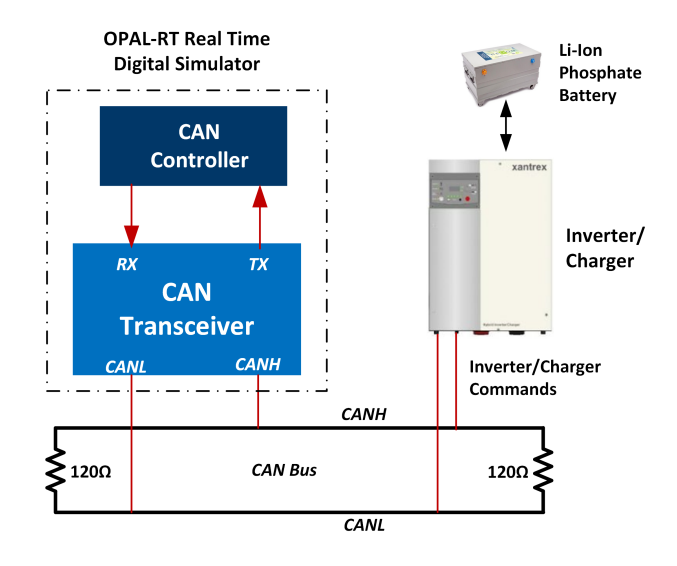


Fig. 3: Block diagram of CAN [8].

B. Charging Command using CAN Communication

In this paper, only the charging mode of the Xantrex inverter/charger unit was used for simplicity. With the generators turned *ON*, the OPAL-RT system was able to send the commands to operate the system in the charging mode. The *ON* and *OFF* commands for the charger were included in their Parameter Group Numbers (PGNs), which were single CAN frames with Data Length Code (DLC) of 3 [12]. Next, to change the charging rate, the charge rate PGN was used to set the charging current. This message has two frames and requires a counter value that matches to the counter on the charger. The counter information was requested through an ISO request. The counter value increments after a new frame of data has been received.

IV. PROCEDURES AND EXPERIMENTAL SETUP

This section describes the experimental setup used for testing the virtual inertia algorithm based on CAN communication. The procedure for setting up the RTDS and the implementation of the virtual inertia algorithm is also described in detail.

A. Equipment Setup

The experimental setup used in this paper is described in Fig. 4. A 10.4 kW generator (Kohler 12RES) sets up a 120/240 AC bus. The generator was equipped with an electronic isochronous governor. The settings of the governor were changed such that the response of the governor was at the slowest setting. This was done so that the generator responds slowly to the changes in the load and the effect of the virtual inertia algorithm is easier to demonstrate. A hybrid inverter/charger (Xantrex XW6048) was also connected to the same AC bus. The DC side of the inverter/charger unit was connected to a 48 V lithium-iron-phosphate battery (from International Battery). A resistive load bank Cannon L-63 was used as a base load for the generator while another resistive load bank was used for load perturbation to test the virtual inertia algorithm. The load bank consisted of steps of resistors that are controlled ON/OFF through a thyristorbased AC voltage controller. An OP5600 RTDS is used as the main controller. The OPAL-RT system sets up the CAN communication with the inverter/charger unit. The voltage and current measurements of the generator are also measured using the OPAL-RT system using at the OP8600 data acquisition system. A PLL was implemented within the OPAL-RT system for the frequency measurements. The parameters of the generator, Xantrex inverter/charger unit and the energy storage system are summarized in Tables I, II, and III respectively.

TABLE I: Kohler 12RES Generator Parameters

THE ELECTRICATE TEXTS OF THE WATER TO A STATE OF THE W	
Fuel Type	Natural gas
Voltage, Frequency	120/240 V, 60 Hz
Governor Type	Electronic
Frequency regulation, No load to Full Load	Isochronous
Frequency regulation, Steady state	±0.5%

TABLE II: Xantrex XW6048 Inverter/Charger Parameters

AC Nominal Power	6000 W
AC Voltage, Frequency	120/240 V, 60 Hz
DC Voltage Range	44-64 VDC

TABLE III: Energy Storage System Parameters

Chemistry	Lithium Iron Phosphate (LiFePo4)
DC Voltage	48 V
Capacity	160 Ah
Maximum Charge Rate	80 A

B. Real-Time Digital Simulator Setup

The virtual inertia control algorithm and the communication was setup in the OP5600 RTDS. The OP5600 system consists

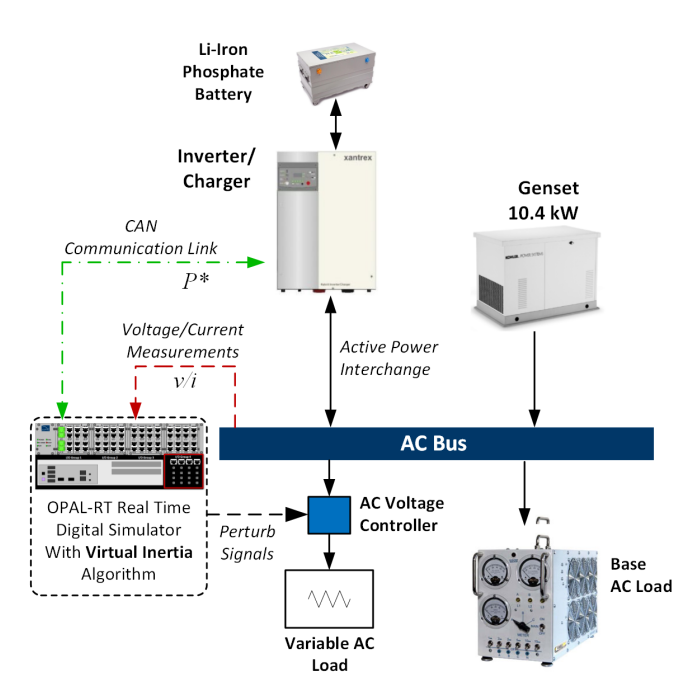


Fig. 4: Schematic diagram of the experimental setup for virtual inertia algorithm. The CAN communication, signal measurements and load perturbation signals are represented by dashed lines.

of an Intel Xeon QuadCore 2.40 GHz CPU with 4 cores as shown in Fig. 5. The virtual inertia algorithm and all the data acquisition was implemented in one of the cores running at a time-step of $T_{s1}=0.0001\ s$. This low time-step was essential for proper performance of the PLL for frequency measurements. The CAN communication was, however, setup in a different core with a higher time-step of $T_{s1}=0.002\ s$ resulting in a multi-rate configuration setup for the test. This allows the CAN communication to run at a higher time-step preventing data overflow. Synchronous data exchange between the cores is performed through shared memory.

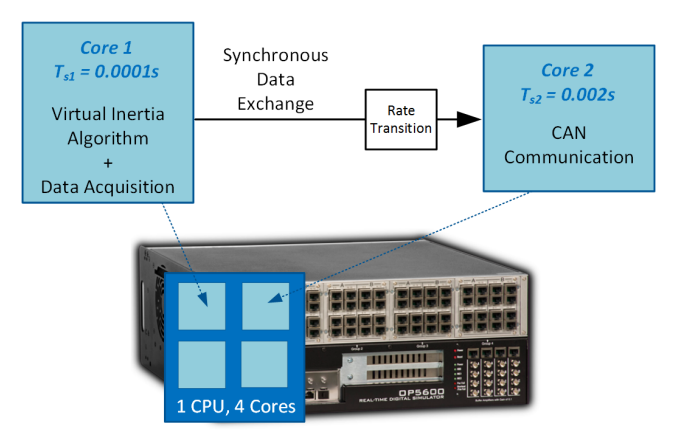


Fig. 5: Schematic diagram of the experimental setup for virtual inertia algorithm.

C. Implementation of Virtual Inertia Control Algorithm

Figure 6 illustrates the implementation of the virtual inertia algorithm in the RTDS. The voltage of the generator is

measured from the data acquisition system and passed into a PLL to measure the frequency. The measured frequency is compared against a reference frequency of 60 Hz. A low pass filter with a cut-off of 15 Hz is implemented to remove the high-frequency noise from the measurements. Figure 7 shows the frequency of the generator with and without the low pass filter. As evident, there is a sustained oscillation of about ± 0.2 Hz in the measured frequency. To prevent the virtual inertia algorithm from responding to these oscillations, a deadline of ± 0.2 Hz is thus implemented. The deadzone, however, adds a further delay in the controller so proper care has to be taken to select this deadzone. The ROCOF is then computed and the power reference is calculated based on (1). The calculated power reference is converted into a current command for the inverter/charger unit based on the DC voltage of the battery.

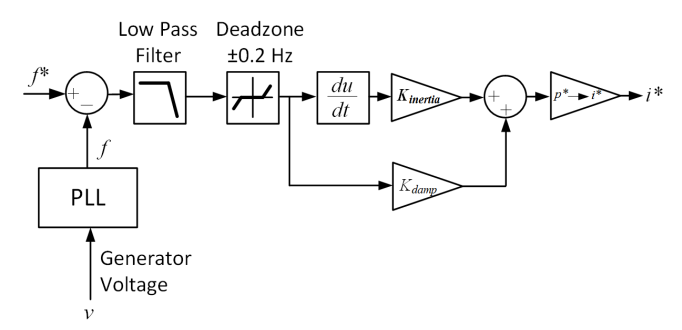


Fig. 6: Implementation of virtual inertia algorithm in OPAL-RT RTDS.

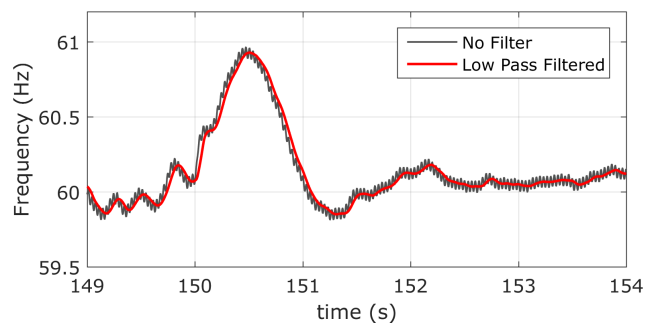


Fig. 7: Generator frequency with and without the low pass filter.

V. RESULTS AND ANALYSIS

The response of the charging current is characterized first in this section followed by testing of the virtual inertia algorithm using the CAN communication protocol. All the measurements are made through the OP8660 data acquisition unit.

A. Current Command Plots

A step current command of 10 A was provided to the inverter/charger unit using the CAN communication setup. The response of the battery charging current to this command is shown in Fig. 8. Initially, even though the current command is 0 A, the battery is charged by a constant DC current of

2 A in the standby mode. This was the default behavior of the Xantrex inverter/charger in the standby mode. When the current command starts at 50 s, there is a delay of 0.4 s before the current starts rising. The current reaches the reference peak current of 10 A after 0.7 s. The ramp rate of the current was measured to be 24.58 A/s. The 0.4 s delay in the actuation of the current command limits the effectiveness of the virtual inertia algorithm as will be described later.

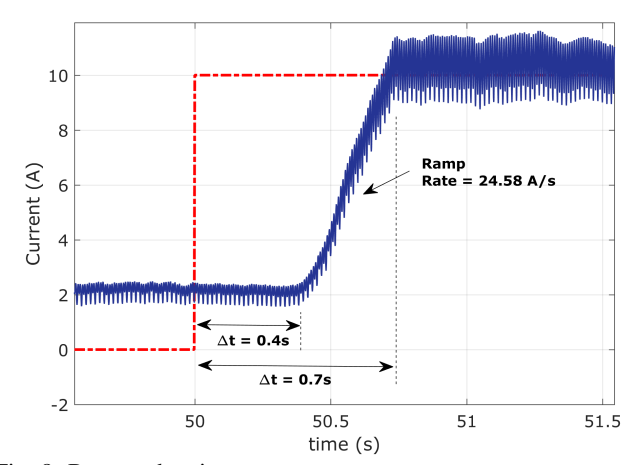


Fig. 8: Battery charging current response.

B. Generator Frequency with Inertial Constant

The frequency of the system for a step decrease in load from 9.9 kW to 8.7 kW is shown in Fig. 9(a). Initially, the Xantrex inverter system with virtual inertia algorithm is not connected to the system. The peak system frequency without the virtual inertia algorithm was 60.95 Hz. Next, to reduce the peak frequency deviation, the Xantrex inverter/charger was connected to the system. In this first test, only the inertial component was used. The inertia constant $k_{inertia}$ was set to 400 and the damping constant k_{damp} was set to 0. The change in frequency was measured by the OPAL-RT RTDS. Current references are then generated which are sent to the Xantrex inverter/charger. The peak frequency with the virtual inertia algorithm was reduced to 60.78 Hz (a reduction of 0.17 Hz). Figure 9(b) shows the slight reduction in the ROCOF of the system with the virtual inertia controller. The active power output of the Xantrex inverter/charger unit is shown in Fig. 9(c). The positive values here indicates the charging of the batteries. There was a significant delay in the actuation of the power. This can be attributed to the delay in the charging current response and the delay introduced due to the deadzone as described earlier.

C. Generator Frequency with Inertial and Damping Constant

In the second test, both the inertia and the damping constant was used. Two sets of experiments were performed. For the first case, $k_{inertia}$ was set to 200 and k_{damp} was set to 50. Similarly, for the second case $k_{inertia}$ was set to 600 and k_{damp} was set to 100. The frequency of the system for these two cases is shown in Fig. 10(a). The frequency

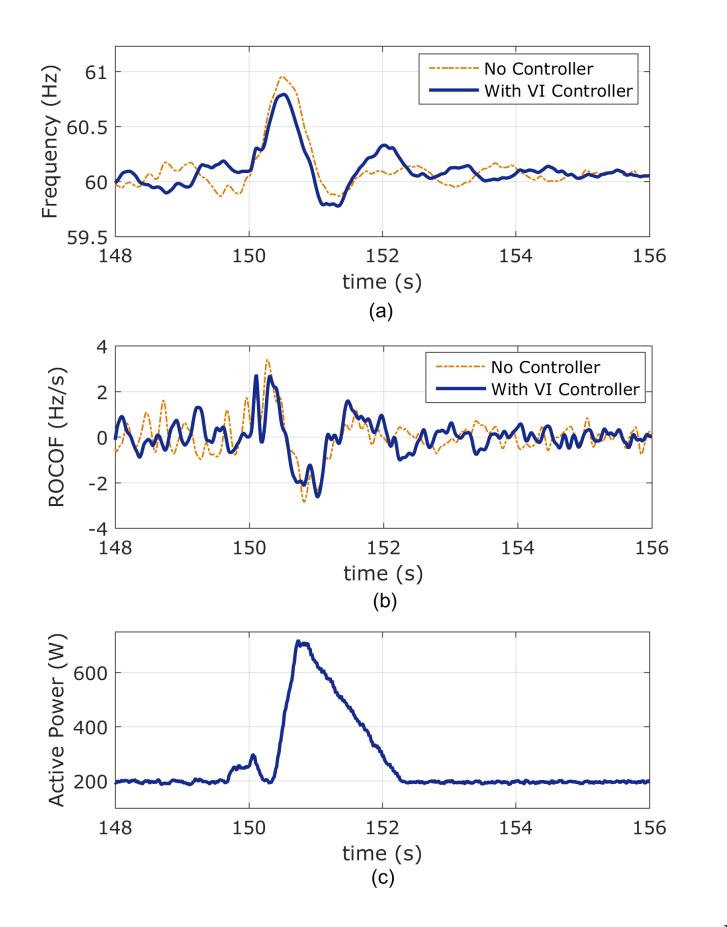


Fig. 9: Experimental results with inertial constant only. (a) Frequency of the generator with and without the virtual inertia controller. (b) ROCOF of the generator. (c)Active power output of the Xantrex inverter/charger unit.

peak was significantly reduced in the second case with the higher gains. The ROCOF and the active power output of the inverter/charger unit are shown in Fig. 10(b) and (c) respectively. Again, the ROCOF was slightly reduced in the cases with virtual inertia. It is interesting to note that the active power output of cases with the lower gain was higher than the case with the higher gains. This was because in the case with the higher gains, the delay in the power response was lower. So, the algorithm was more effective in reducing the frequency earlier thus requiring less power.

VI. CONCLUSIONS AND FUTURE WORK

A virtual inertia algorithm was implemented in a commercial off-the-self inverter in this paper. CAN (or another form of communication) can be a cost-effective measure to retrofit existing inverters with virtual inertia control. A number of delays existed in the system. For instance, the delay due to the communication latency, delay in current actuation and the requirement of the deadzone for oscillatory frequency measurements. All these reasons prevented the setup from showing the desired behavior. Even though the CAN-based communication had significant delays the virtual inertia algorithm was, however, able to reduce the frequency variations

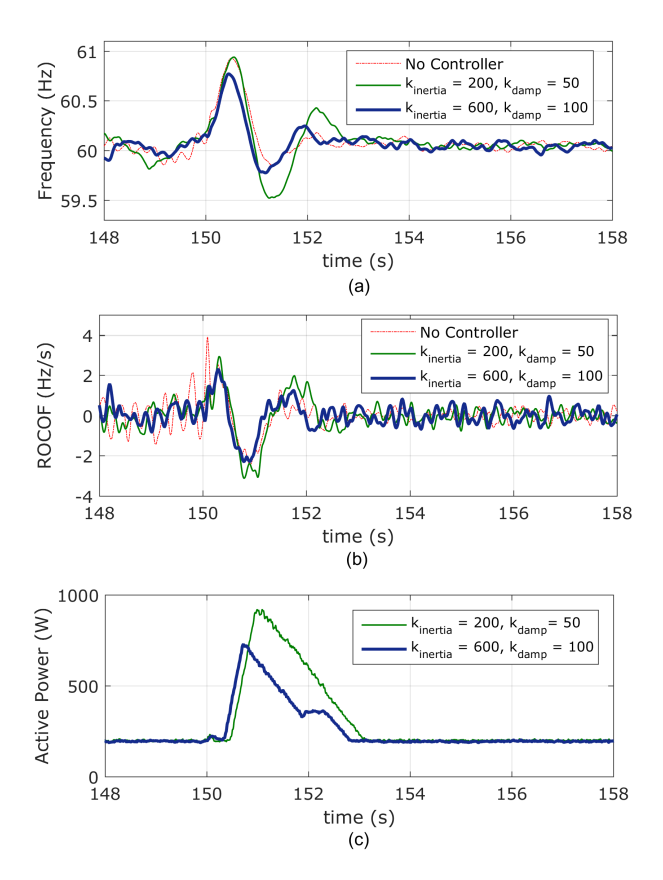


Fig. 10: Experimental results with both inertial and damping constant. (a) Frequency of the generator with and without the virtual inertia controller. (b) ROCOF of the generator. (c)Active power output of the Xantrex inverter/charger unit..

in the system to some extent. For future work, other forms of communication will be explored which may provide a lower latency. Furthermore, the modeling of the generator can also be explored so that the gains of the virtual inertia controller can be better tuned.

ACKNOWLEDGMENT

The authors would like to acknowledge the NSF MRI Grant No. 1726964. The authors would also like to acknowledge OPAL-RT Technologies for the technical support in implementing the experimental setup. The authors would also like to thanks Shaili Nepal, Dan Flaskey and Ryan Johnson for their assistance in setting up the CAN communication and running the experiments.

REFERENCES

- U. Tamrakar, D. Shrestha, M. Maharjan, B. P. Bhattarai, T. M. Hansen, and R. Tonkoski, "Virtual inertia: Current trends and future directions," *Applied Sciences*, vol. 7, no. 7, p. 654, 2017.
- [2] H.-P. Beck and R. Hesse, "Virtual synchronous machine," in 9th IEEE International Conference on Electrical Power Quality and Utilisation, 2007, 6 pp.
- [3] Q.-C. Zhong and G. Weiss, "Synchronverters: Inverters that mimic synchronous generators," *IEEE Transactions on Industrial Electronics*, vol. 58, no. 4, pp. 1259–1267, 2011.

- [4] K. Sakimoto, Y. Miura, and T. Ise, "Stabilization of a power system with a distributed generator by a virtual synchronous generator function," in 8th IEEE International Conference on Power Electronics and ECCE Asia, 2011, pp. 1498–1505.
- [5] J. M. Guerrero, L. G. de Vicuna, J. Matas, M. Castilla, and J. Miret, "A wireless controller to enhance dynamic performance of parallel inverters in distributed generation systems," *IEEE Trans. Power Electron.*, vol. 19, no. 5, pp. 1205–1213, Sept 2004.
- [6] J. Kim, J. M. Guerrero, P. Rodriguez, R. Teodorescu, and K. Nam, "Mode adaptive droop control with virtual output impedances for an inverter-based flexible ac microgrid," *IEEE Trans. Power Electron.*, vol. 26, no. 3, pp. 689–701, March 2011.
- [7] Reciprocating internal combustion engine driven alternating current generating sets- Part 5: Generating sets, Std. ISO 8528-5:2005(E), 2005.
- [8] S. Nepal, A. Shakya, R. Fourney, J. Sternhagen, and R. Tonkoski,

- "Development of real-time control of commercial off-the-shelf inverter/charger for energy management of microgrids," in *IEEE Power and Energy Society General Meeting (PESGM), 2016*, 2016, pp. 1–5.
- [9] U. Tamrakar, D. Galipeau, R. Tonkoski, and I. Tamrakar, "Improving transient stability of photovoltaic-hydro microgrids using virtual synchronous machines," in *IEEE Eindhoven PowerTech*, 2015, 6 pp.
- [10] R. I. Davis, A. Burns, R. J. Bril, and J. J. Lukkien, "Controller area network (CAN) schedulability analysis: Refuted, revisited and revised," *Real-Time Systems*, vol. 35, no. 3, pp. 239–272, 2007.
- [11] L. Wolfhard, "CAN system engineering: From theory to practical application," 1997.
- [12] S. Nepal, "Development of microgrid test bed for testing energy management system"," Master's thesis, South Dakota State University (SDSU), 2017.